



# Analysis of Cattaneo–Christov theory for unsteady flow of Maxwell fluid over stretching cylinder

Masood Khan<sup>1</sup> · Awais Ahmed<sup>1</sup> · Muhammad Irfan<sup>1</sup> · Jawad Ahmed<sup>1,2</sup>

Received: 18 November 2019 / Accepted: 13 January 2020 / Published online: 14 February 2020  
© Akadémiai Kiadó, Budapest, Hungary 2020

## Abstract

Analysis of thermal and solutal energy transport phenomena in Maxwell fluid flow with the help of Cattaneo–Christov double diffusion theory is performed in this article. Unsteady 2D flow of Maxwell fluid with variable thermal conductivity over the stretching cylinder is considered here. We formulate the partial differential equations (PDEs) under given assumptions for the governing physical problem of heat and mass transport in Maxwell fluid by using double diffusion of Cattaneo–Christov model rather than classical Fourier’s and Fick’s law. Numerical technique *bvp4c* is employed for the solution of ordinary differential equations (ODEs) which are obtained from governing PDEs under the appropriate similarity transformations. In the view of acquired results, we observed that for convenient results the values of unsteadiness parameter should be less than one. The higher values of Maxwell parameter declines the flow field but increase the energy transport in the fluid flow. Both temperature and concentration distributions in Maxwell liquid decline for higher values of thermal and concentration relaxation time parameter. Moreover, small thermal conductivity parameter also enhances the temperature field. The validation of results is proved with the help of comparison Table 1 with previous articles. The present results are found with help of *bvp4c* scheme and homotopy analysis method (HAM).

**Keywords** Transient flow · Cattaneo–Christov model · Maxwell fluid · Variable thermal conductivity · *Bvp4c*

## Introduction

Nowadays researchers paid too much attention in the analysis of heat and mass transfer due to their plenteous applications in the field of engineering and industrial appliances such as cooling of nuclear reactor, heat exchanger, refrigerator, polymer process, plastics extrusion. Fourier’s and Fick’s laws are the basic fundamental mathematical relations which are used to describe the mechanism of the transport of heat and mass in given medium due to temperature and concentration difference, respectively. Fourier’s law lead to parabolic-type equation for the temperature field which means heat transport has infinite speed and propagate throughout the medium with initial disturbance. To resolve this heat transport paradox, the Fourier’s law needs the some modifications. Many

attempts have taken to clear up this paradox but not at all have been successful. Cattaneo [1] modified the Fourier’s law by introducing the thermal relaxation time parameter multiply with time derivative of heat flux which yields to the hyperbolic-type equation for heat transport phenomenon and as results, transport of heat has finite speed in the entire medium. This new model termed as Maxwell–Cattaneo (MC) model. In order to make this model frame invariant, Christov [2] amend the MC model by replacing time derivative to upper-convective time derivative which includes the higher spatial gradients. Yousif et al. [3] numerically studied the momentum and heat transport by using Fourier’s law in the flow Carreau nanofluid under the influence of magnetic field and internal sink/source. Sarafraz et al. [4] examined the characteristics of heat transport by employing Fourier’s law of heat conduction in the process of pool boiling in the presence of constant magnetic field.

Recently, scientists explored the heat and mass transport phenomena by using the Cattaneo–Christov double diffusion theory for the flow of both Newtonian and non-Newtonian fluids in different geometries. Han et al. [5] studied the flow of viscoelastic fluid with the impact of

✉ Jawad Ahmed  
j.ahmed@math.qau.edu.pk

<sup>1</sup> Department of Mathematics, Quaid-i-Azam University, Islamabad 44000, Pakistan

<sup>2</sup> Department of Basic Sciences, University of Engineering and Technology, Taxila 47050, Pakistan

Cattaneo–Christov theory. They found the graphical outcomes for temperature and concentration fields. MHD flow of viscous fluid with Cattaneo–Christov model over the stretching sheet was explored by Upadhyaya et al. [6] Reduction in the heat transfer is observed for higher values of thermal relaxation parameter. Cattaneo–Christov double diffusion theory employed to the rotating flow of Oldroyd-B fluid over the stretching sheet with variable thermal conductivity by Khan et al. [7] Numerical investigation was performed by Ibrahim [8] on the 3D rotating flow of Powell-Eyring fluid and heat transfer with the help of non-Fourier’s law. Farooq et al. [9] analyzed the Cattaneo–Christov theory for the flow of viscous fluid with variable thermal conductivity and mass diffusivity. Their results revealed that both temperature and concentration fields decline for thermal and mass relaxation time parameters. Alamri et al. [10] investigated the flow of second-grade fluid over stretching cylinder with the perspective of Cattaneo–Christov heat flux model. Furthermore, numerous investigation has been performed for the analysis of Fourier’s law and Cattaneo–Christov double diffusion theory for the heat transport in the flow of various fluid models (see Refs. [11–20]). In the recent study of heat transfer enhancement, Khan et al. [21] scrutinized the effect of nanoparticles with different shapes in the peristaltic MHD flow of nanofluid.

Due to wide range applications of non-Newtonian fluids in engineering process attracted the researchers to investigate their perplexing rheology and also transport of thermal and solutal energy behaviors. Many engineering equipments used the non-Newtonian fluids, e.g., for reduction in friction in oil-pipe line, soldiers suits fill with some non-Newtonian fluids that turns into solid when built hit them, use as surfactant for large-scale heating and cooling systems, use in manufacturing lubricants for vehicles. As non-Newtonian fluids change their flow behavior under the applied stress, thus the researchers give various empirical models to describe the behavior of the non-Newtonian fluids. The constitutive equations for flow are highly complicated and nonlinear. The numerous analytical and numerical techniques are employed to tackle the flow equations for these nonlinear fluids. Raju et al. [22] studied the flow of non-Newtonian nanofluid over the cone under the influence of magnetic field. Flow of Maxwell fluid with heat transport with the influence of viscous dissipation and radiation was analyzed by Hsiao [23]. Application of Carreau nanofluid flow to enhance the heat transport in thermal extrusion manufacturing system was explored by Hsiao [24]. Ahmed et al. [25] numerically investigated the stagnation point flow of Maxwell fluid over the permeable rotating and stretching disk, and their results revealed that radial velocity increases with higher values of velocity ratio parameter. Moshkin et al.

[26] analyzed the transient stagnation point 2D flow of Maxwell fluid.

In the subject of fluid dynamics, the flow of various fluid models with different dynamical properties induced by stretching surfaces attract the researcher to investigate its characteristics due to its diverse applications in engineering mechanism such as wire drawing, glass fiber, hot rolling, paper production, etc. In a wide range of applications such as plastic extrusion process flow over stretching cylinders is also critically important. Hsiao [27] investigated the mixed convection stagnation point flow over stretching sheet with slip boundary condition under the impact of uniform magnetic field. Numerical results were obtained by using finite difference scheme (FDM). The higher rate of heat transport was observed in case of more value of stagnation parameter. Flow of MHD micropolar fluid induced above the stretching sheet in addition to viscous dissipation was studied by Hsiao [28]. Application of Darcy–Forchheimer law to the flow nanofluid over curved stretching surface was investigated by Saif et al. [29]. The outcomes revealed that skin friction coefficient boosts up for higher porosity parameter and inertia coefficient. Ahmed et al. [30] numerically studied the unsteady flow of CNT nanofluid over shrinking surface by considering the variable viscosity of fluid and heat transport in it.

In view of the above detailed studies, we proposed this note to investigate the heat and mass transport in Maxwell fluid flow over the stretched cylinder in unsteady state. For the formation of energy and concentration equations, we utilize the Cattaneo–Christov double diffusion theory. Numerical solutions with the help of `bvp4c` function are obtained for governing physical problem. The outcomes for velocity, temperature and concentration fields are presented graphically and discussed in detail with the help of physical justification.

## Mathematical formulation

Consider the unsteady laminar 2D flow of an incompressible Maxwell fluid with variable thermal conductivity influenced by stretching cylinder of radius  $R_1$ . Suppose that  $u$  and  $w$  are velocity components along  $z$ -axis (axis of cylinder) and  $r$ -axis (normal to  $z$ -axis), respectively as presented in Fig. 1. The time-dependent stretching velocity of the cylinder is assumed to be  $u_w(t, z) = \frac{az}{1-\gamma t}$  where  $a, \gamma > 0$ . Thermal and solutal energy transport in the flow is conducted by using Cattaneo–Christov double diffusion theory. The Maxwell fluid model is defined as [31]

$$\left(1 + \lambda_1 \frac{D}{Dt}\right) \mathbf{S} = \mu \mathbf{A}_1, \quad (1)$$

where  $\lambda_1$  is the relaxation time,  $\frac{D}{Dt}$  signifies the Oldroyd derivative,  $S$  the extra stress tensor,  $\mathbf{A}_1 = \nabla\mathbf{V} + (\nabla\mathbf{V})^T$  the first Rivlin–Erickson tensor and  $\mu$  the viscosity of the fluid. If  $\lambda_1 = 0$  in Eq. (1) we recover the Newtonian fluid model.

The Cattaneo–Christov model for conduction of heat and mass are used rather than classical Fourier’s and Fick’s laws. If  $\mathbf{q}$  and  $\mathbf{J}$  are heat and mass fluxes, respectively, then both satisfy the following mathematical expressions [9, 10]

$$\mathbf{q} + \lambda_t \left( \frac{\partial \mathbf{q}}{\partial t} + \mathbf{V} \cdot \nabla \mathbf{q} + (\nabla \mathbf{V}) \mathbf{q} - \mathbf{q} \cdot \nabla \mathbf{V} \right) = -K(T) \nabla T, \tag{2}$$

$$\mathbf{J} + \lambda_c \left( \frac{\partial \mathbf{J}}{\partial t} + \mathbf{V} \cdot \nabla \mathbf{J} + (\nabla \cdot \mathbf{V}) \mathbf{J} - \mathbf{J} \cdot \nabla \mathbf{V} \right) = -D_B \nabla C. \tag{3}$$

In the above equations  $\lambda_t$  is the thermal time relaxation and  $\lambda_c$  the mass time relaxation,  $K(T) = k_\infty(1 + \epsilon\theta)$  the variable thermal conductivity ( $k_\infty$  free stream conductivity,  $\epsilon$  small conductivity parameter and  $\theta$  the dimensionless temperature) and  $D_B$  the Brownian diffusion coefficient. If  $\lambda_t = \lambda_c = 0$  then both Eqs. (2) and (3) reduce to classical Fourier’s and Ficks’s laws, respectively. For an incompressible fluid, Eqs. (2) and (3) become

$$\mathbf{q} + \lambda_t \left( \frac{\partial \mathbf{q}}{\partial t} + \mathbf{V} \cdot \nabla \mathbf{q} - \mathbf{q} \cdot \nabla \mathbf{V} \right) = -K(T) \nabla T, \tag{4}$$

$$\mathbf{J} + \lambda_c \left( \frac{\partial \mathbf{J}}{\partial t} + \mathbf{V} \cdot \nabla \mathbf{J} - \mathbf{J} \cdot \nabla \mathbf{V} \right) = -D_B \nabla C. \tag{5}$$

The basic transport equations for flow, heat and mass transport found by conservation laws are

$$\rho \frac{d\mathbf{V}}{dt} = -\nabla p + \nabla \cdot \mathbf{S}, \tag{6}$$

$$(\rho c_p) \frac{dT}{dt} = -\nabla \cdot \mathbf{q}, \tag{7}$$

$$\frac{dC}{dt} = -\nabla \cdot \mathbf{J}. \tag{8}$$

By applying the law of conservation of mass, momentum and energy to the whole system of flow problem and eliminating  $\mathbf{S}$  in Eqs. (1) and (6),  $\mathbf{q}$  in Eqs. (2) and (7) and  $\mathbf{J}$  in Eqs. (3) and (8), respectively, we arrived at following set of governing partial differential equations (Fig. 1):

$$\frac{\partial(ru)}{\partial z} + \frac{\partial(rw)}{\partial r} = 0, \tag{9}$$

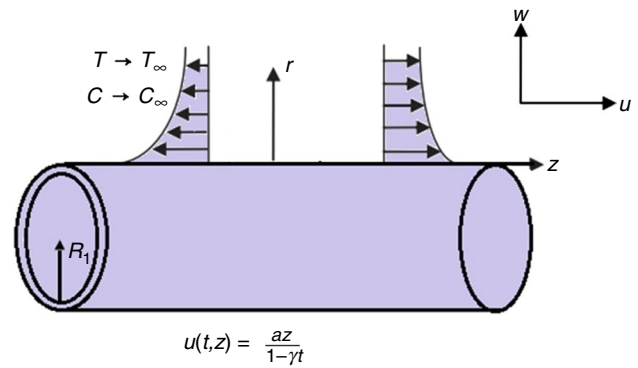


Fig. 1 Flow configuration and coordinate system

$$\begin{aligned} \frac{\partial u}{\partial t} + u \frac{\partial u}{\partial z} + w \frac{\partial u}{\partial r} = v \left[ \frac{\partial^2 u}{\partial r^2} + \frac{1}{r} \frac{\partial u}{\partial r} \right] \\ - \lambda_1 \left[ \frac{\partial^2 u}{\partial t^2} + 2u \frac{\partial^2 u}{\partial t \partial z} + 2w \frac{\partial^2 u}{\partial r \partial t} + 2uw \frac{\partial^2 u}{\partial r \partial z} \right. \\ \left. + w^2 \frac{\partial^2 u}{\partial r^2} + u^2 \frac{\partial^2 u}{\partial z^2} \right], \end{aligned} \tag{10}$$

$$\begin{aligned} \frac{\partial T}{\partial t} + u \frac{\partial T}{\partial z} + w \frac{\partial T}{\partial r} + \lambda_t \\ \left[ \frac{\partial^2 T}{\partial t^2} + \frac{\partial u}{\partial t} \frac{\partial T}{\partial z} + 2u \frac{\partial^2 T}{\partial t \partial z} \right. \\ \left. + \frac{\partial w}{\partial t} \frac{\partial T}{\partial r} + 2w \frac{\partial^2 T}{\partial t \partial r} + 2uw \frac{\partial^2 T}{\partial r \partial z} \right. \\ \left. + w^2 \frac{\partial^2 T}{\partial r^2} + u^2 \frac{\partial^2 T}{\partial z^2} + u \frac{\partial u}{\partial z} \frac{\partial T}{\partial z} \right. \\ \left. + w \frac{\partial w}{\partial r} \frac{\partial T}{\partial r} + u \frac{\partial w}{\partial z} \frac{\partial T}{\partial r} + w \frac{\partial u}{\partial r} \frac{\partial T}{\partial r} \right] \\ = \frac{1}{(\rho c_p)_f} \frac{1}{r} \frac{\partial}{\partial r} \left[ K(T) \left( r \frac{\partial T}{\partial r} \right) \right], \end{aligned} \tag{11}$$

$$\begin{aligned} \frac{\partial C}{\partial t} + u \frac{\partial C}{\partial z} + w \frac{\partial C}{\partial r} + \lambda_c \\ \left[ \frac{\partial^2 C}{\partial t^2} + \frac{\partial u}{\partial t} \frac{\partial C}{\partial z} + 2u \frac{\partial^2 C}{\partial t \partial z} + \frac{\partial w}{\partial t} \frac{\partial C}{\partial r} \right. \\ \left. + 2w \frac{\partial^2 C}{\partial t \partial r} + 2uw \frac{\partial^2 C}{\partial r \partial z} \right. \\ \left. + w^2 \frac{\partial^2 C}{\partial r^2} + u^2 \frac{\partial^2 C}{\partial z^2} + u \frac{\partial u}{\partial z} \frac{\partial C}{\partial z} \right. \\ \left. + w \frac{\partial w}{\partial r} \frac{\partial C}{\partial r} + u \frac{\partial w}{\partial z} \frac{\partial C}{\partial r} + w \frac{\partial u}{\partial r} \frac{\partial C}{\partial r} \right] \\ = D_B \frac{1}{r} \frac{\partial}{\partial r} \left[ \left( r \frac{\partial C}{\partial r} \right) \right]. \end{aligned} \tag{12}$$

The corresponding boundary conditions for given problems are

$$\begin{aligned} u(t, z, r) = u_w(t, z) = \frac{az}{1 - \gamma t}, \quad w(t, z, r) = 0, \\ T = T_w, \quad C = C_w \quad \text{at } r = R_1, \end{aligned} \tag{13}$$

$$u \rightarrow 0, \quad T \rightarrow T_\infty, \quad C \rightarrow C_\infty \quad \text{as } r \rightarrow \infty. \tag{14}$$

Here  $\nu$  is the kinematic viscosity,  $T_w$  and  $C_w$  are temperature and concentration at the wall, respectively,  $T_\infty$  and  $C_\infty$  the free stream temperature and concentration, respectively,  $\rho$  the fluid density and  $c_p$  the specific heat capacity at constant pressure.

With the help of following conversion parameters

$$\begin{aligned} u &= -\frac{R_1}{r} \sqrt{\frac{av}{1-\gamma t}} f(\eta), & w &= \frac{az}{1-\gamma t} f'(\eta), \\ \theta(\eta) &= \frac{T - T_\infty}{T_w - T_\infty} \\ \phi(\eta) &= \frac{C - C_\infty}{C_w - C_\infty}, & \eta &= \sqrt{\frac{a}{\nu(1-\gamma t)}} \left( \frac{r^2 - R_1^2}{2R_1} \right), \end{aligned} \tag{15}$$

Equation (9) is satisfied automatically and Eqs. (10)–(14) yield

$$\begin{aligned} (1 + 2\alpha\eta)f'''' + 2\alpha ff'' - \frac{S}{2}\eta f'' - Sf' - f'^2 \\ + ff'' - \frac{7}{4}\beta_1 S^2 \eta f'' \\ - \frac{\beta_1}{4}\eta^2 S^2 f'' - 2\beta_1 S^2 f' - 2S\beta_1 f'^2 - \beta_1 \eta S f' f'' \\ + S\beta_1 \eta f f'' \\ + 3S\beta_1 ff'' + 2\beta_1 ff' f'' - \frac{\alpha\beta_1}{1+2\alpha\eta} f^2 f'' \\ - \beta_1 f^2 f'' = 0, \end{aligned} \tag{16}$$

$$\begin{aligned} (1 + 2\alpha\eta)\theta'' + \text{Pr} \left( f\theta' - \frac{S}{2}\eta\theta' \right) + (1 + 2\alpha\eta)(\theta\theta'' + \theta'^2)\epsilon \\ + 2\alpha\theta' + 2\alpha\epsilon\theta\theta' - \text{Pr} \beta_1 \left( \frac{3}{4}S^2\eta\theta' - \frac{3S}{2}\theta'f - \frac{S}{2}\eta\theta'f' \right. \\ \left. + \frac{1}{4}S^2\eta^2\theta'' - S\eta f\theta'' + \theta''f^2 + \theta'ff' \right) = 0, \end{aligned} \tag{17}$$

$$\begin{aligned} (1 + 2\alpha\eta)\phi'' + \text{Le Pr} \left( f\phi' - \frac{S}{2}\eta\phi' \right) + 2\alpha\phi' \\ - \text{Le Pr} \beta_c \left( \frac{3}{4}S^2\eta\phi' - \frac{3S}{2}\phi'f - \frac{S}{2}\eta\phi'f' \right. \\ \left. + \frac{1}{4}S^2\eta^2\phi'' - S\eta f\phi'' + \phi''f^2 + \phi'ff' \right) = 0, \end{aligned} \tag{18}$$

$$f(0) = 0, \quad f'(0) = 1, \quad \theta(0) = 1, \quad \phi(0) = 1, \tag{19}$$

$$f'(\infty) = 0, \quad \theta(\infty) = 0, \quad \phi(\infty) = 0. \tag{20}$$

In the above equations  $S$  ( $= \frac{\gamma}{a}$ ) is the unsteadiness parameter,  $\alpha$  ( $= \frac{1}{R_1} \sqrt{\frac{\nu(1-\gamma t)}{a}}$ ) the curvature parameter,  $\beta_1$  ( $= \frac{\lambda_1 a}{1-\gamma t}$ ) the Maxwell parameter,  $\text{Pr}$  ( $= \frac{\nu}{\alpha_1}$ ) the Prandtl number,  $\beta_t$

( $= \frac{\lambda_1 a}{1-\gamma t}$ ) the thermal relaxation time parameter,  $\beta_c$  ( $= \frac{\lambda_c a}{1-\gamma t}$ ) the mass relaxation time parameter and  $\text{Le}$  ( $= \frac{\alpha_1}{D_B}$ ) the Lewis number.

### Solution procedure

This section is proposed for the solution of established ODEs for flow, energy and concentration Eqs. (16), (17) and (18) along with corresponding boundary conditions given in Eqs. (19) and (20) the numerically. Bvp4c built in MATLAB technique is used to acquire the numerical results. For this we transformed the governing ODEs to the system of first-order ordinary differential equations. For this, we used the transformed variables as

$$f = y_1, \quad f' = y_2, \quad f'' = y_3, \quad f''' = yy_1, \tag{21}$$

$$\theta = y_4, \quad \theta' = y_5, \quad \theta'' = yy_2, \tag{22}$$

$$\phi = y_6, \quad \phi' = y_7, \quad \phi'' = yy_3. \tag{23}$$

The resulting first-order ODEs are as follows

$$yy_1 = \frac{y_2^2 - y_1 y_3 + S y_2 + \frac{S}{2} \eta y_3 - 2\alpha y_1 y_3 + \frac{7}{4} \beta_1 S^2 \eta y_3 + 2\beta_1 S^2 y_2 + 2\beta_1 S y_1^2 + \beta_1 \eta S y_1 y_3 - 3\beta_1 S y_1 y_3 - 2\beta_1 y_1 y_2 y_3 + \frac{\alpha \beta_1}{1+2\alpha\eta} y_1^2 y_3}{a_1}, \tag{24}$$

$$yy_2 = \frac{\text{Pr} \beta_t \left( y_1 y_2 y_5 - \frac{3}{2} S y_5 y_1 - \frac{S}{2} \eta y_2 y_5 + \frac{3}{4} S^2 \eta y_5 \right) + \text{Pr} \left( \frac{S}{2} \eta y_5 - y_1 y_5 \right) - 2\alpha y_5}{a_2}, \tag{25}$$

$$yy_3 = \frac{\text{Le Pr} \beta_c \left( y_1 y_2 y_7 - \frac{3}{2} S y_1 y_7 - \frac{S}{2} \eta y_2 y_7 + \frac{3}{4} S^2 \eta y_7 \right) + \text{Le Pr} \left( \frac{S}{2} \eta y_7 - y_1 y_7 \right) - 2\alpha y_7}{a_3}, \tag{26}$$

where

$$\begin{aligned} a_1 &= 1 + 2\alpha\eta - \frac{\beta_1}{4}\eta^2 S^2 + S\beta_1 \eta y_1 - \beta_1 y_1^2, \\ a_2 &= 1 + 2\alpha\eta - \frac{\text{Pr}}{4}\beta_t S^2 \eta^2 \\ &\quad + \beta_t S \text{Pr} \eta y_1 + (1 + 2\alpha\eta)\epsilon y_4 - \text{Pr} \beta_t y_1^2, \\ a_3 &= 1 + 2\alpha\eta - \frac{\text{Le Pr}}{4}\beta_c S^2 \eta^2 + \text{Le Pr} S \text{Pr} \eta y_1 - \text{Le Pr} \beta_c y_1^2. \end{aligned}$$

Boundary conditions for the above first-order differential system are

$$y_1(0) = 0, \quad y_2(0) = 1, \quad y_4(0) = 1, \quad y_6(0) = 1, \quad (27)$$

$$y_2(\infty) = 0, \quad y_4(\infty) = 0, \quad y_6(\infty) = 0. \quad (28)$$

### Discussion of results

The flow velocity, temperature distribution and mass transport in Maxwell liquid are the key points of our analysis. Impact of pertinent parameters with following fixed values  $S = \epsilon = 0.01$ ,  $\beta_1 = \beta_t = \beta_c = 0.5$ ,  $Pr = 6.5$ ,  $Le = 6.5$  on the velocity, temperature and concentration fields are presented graphically with the comparison of cylinder and sheet. It is observed that there is higher energy transport in case of cylinder than sheet. Figure 2a–c explores the impact of curvature parameter on velocity, temperature and concentration, respectively. For higher values of curvature parameter  $\alpha$ , we noted the increasing trend in velocity, temperature and concentration fields. Physically,

higher value of  $\alpha$  reduces the radius of cylinder; thus, the influence of boundary in fluid motion decreases. Hence as result velocity of fluid increases and corresponding heat and mass transport in the fluid enhance. The increasing trend is observed for temperature and concentration fields for growing values of Maxwell parameter  $\beta_1$ . The adverse behavior is found in case of flow field as shown in Fig. 3a–c. Physically, the Maxwell parameter  $\beta_1$  describes the rheology of viscoelastic-type material. The Maxwell parameter  $\beta_1$  is the dimensionless relaxation time. The relaxation time is used to depict the phenomena of stress relaxation and stress relaxation (retain in deformation of material after sudden applied stress) observed due to elasticity of material. Therefore, material for higher value of  $\beta_1$  behaves like a solid. It means the more time is required for material to retain its deformation, thus, in result the decline in fluid velocity is observed due to higher value of  $\beta_1$ . On the other hand, energy transport phenomenon boost up for same trend of  $\beta_1$  due to increase in heat conduction rate. Plots in Fig. 4a, b described the effect of unsteadiness

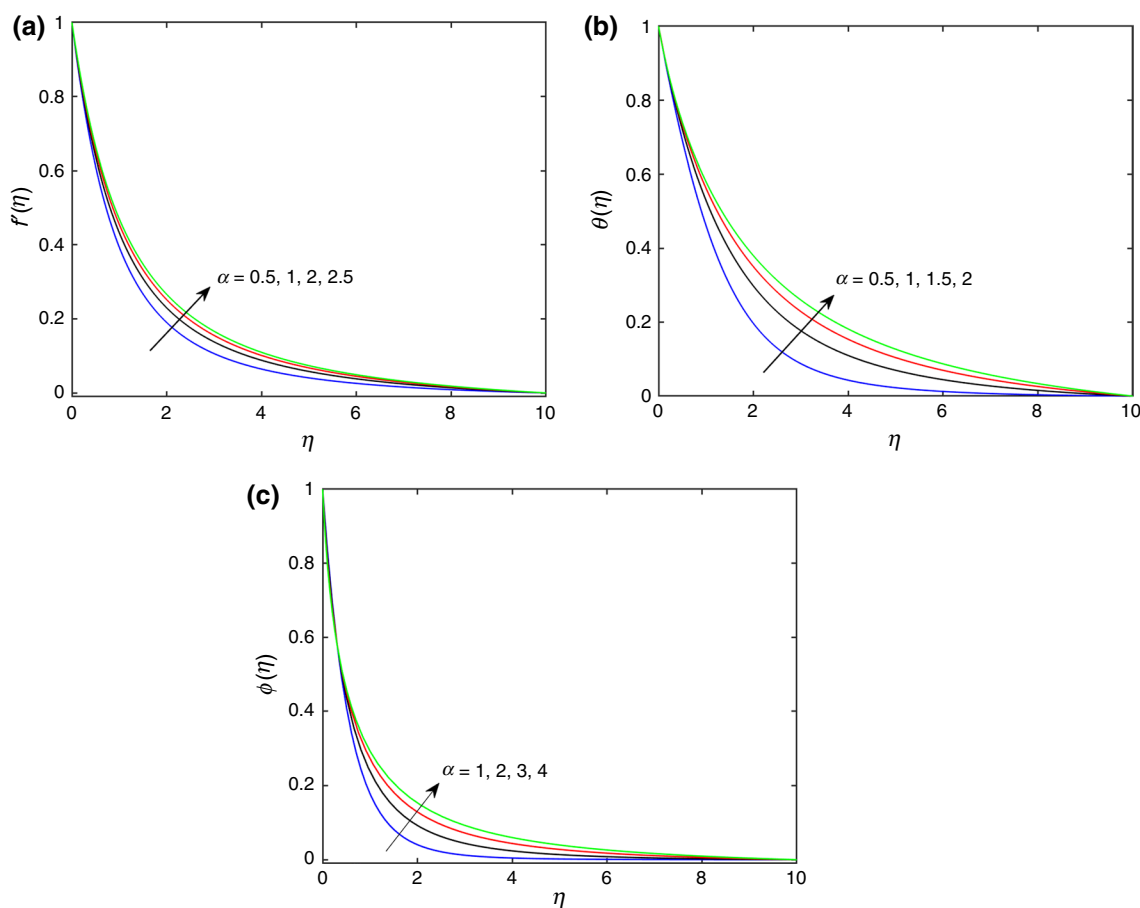
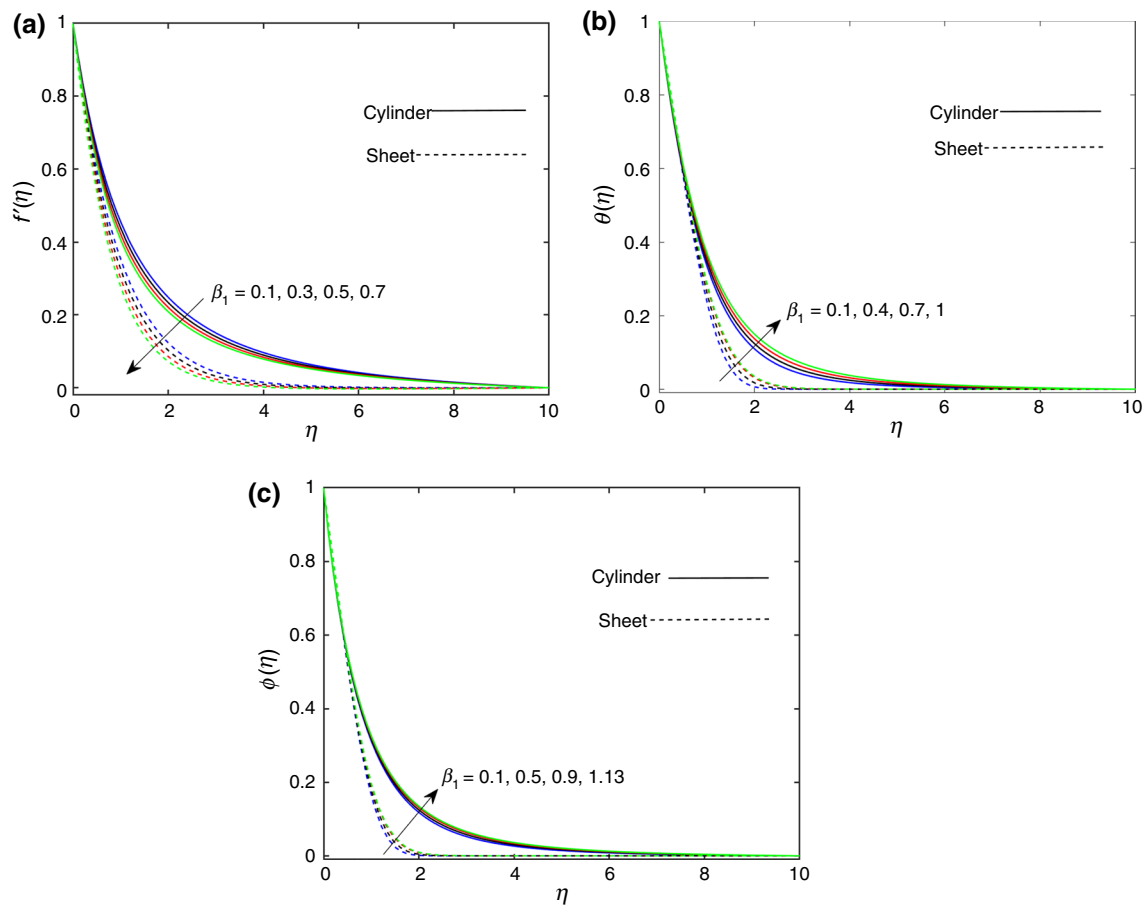
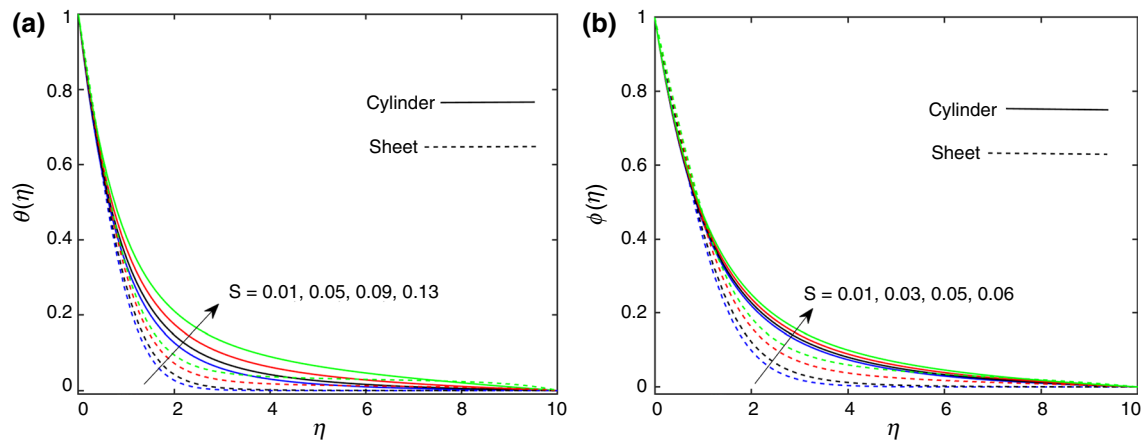


Fig. 2 a–c The velocity, temperature and concentration profiles via curvature parameter  $\alpha$



**Fig. 3** a–c The velocity, temperature and concentration profiles via Maxwell parameter  $\beta_1$



**Fig. 4** a, b The temperature and concentration profiles via unsteadiness parameter  $S$

parameter  $S$  on heat and mass transportation mechanisms. Both the temperature and concentration fields boost up for increasing values of  $S$ . Figure 5a, b is sketched to depict

the impact on heat and mass transfer rate of thermal and mass relaxation time parameters  $\beta_t$  and  $\beta_c$ . Increasing values of both thermal relaxation time and solutal relaxation

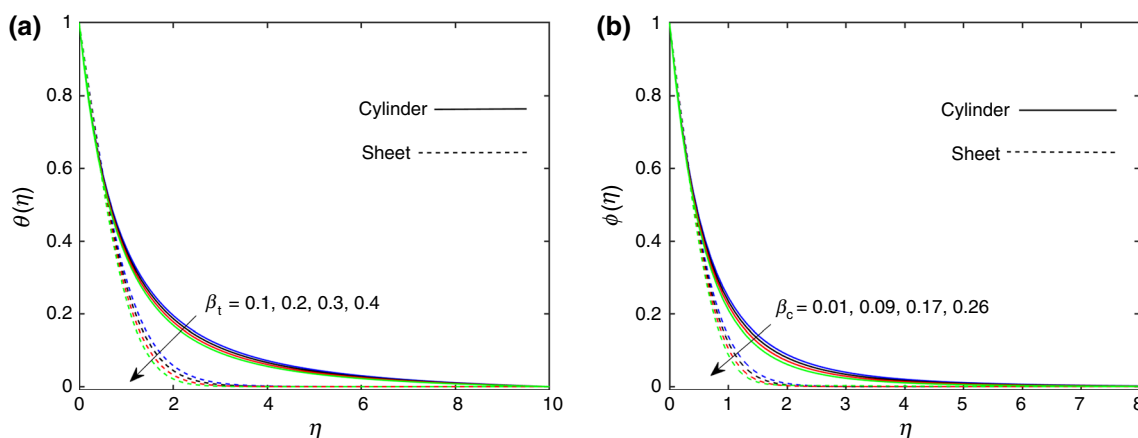


Fig. 5 a, b The temperature and concentration profiles via  $\beta_t$  and  $\beta_c$ , respectively

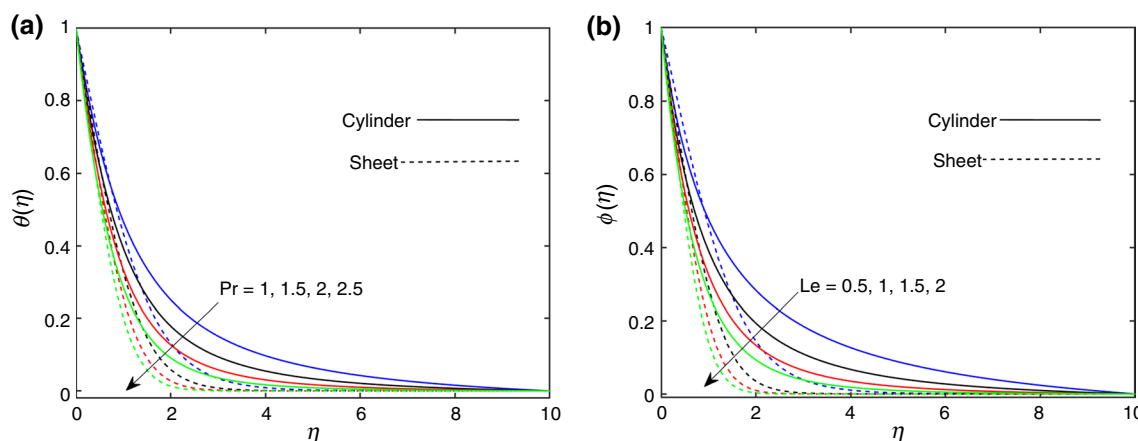


Fig. 6 a, b The temperature and concentration profiles via Prandtl number Pr and Lewis number Le, respectively

time parameter declines the temperature and concentration fields, respectively. Physically, higher values of relaxation time parameter in Cattaneo–Christov heat flux model control the instant propagation of heat waves in given medium. Therefore, the fluid with enlarging value of relaxation time parameters required more time for the transport of heat and mass. Consequently, the temperature and concentration fields decrease. The relative importance of momentum, thermal and mass diffusivity is described by Prandtl number Pr and Lewis number Le. Figure 6a, b is indicated to show the variation in temperature and concentration profiles via Prandtl and Lewis numbers, respectively. We conclude that both temperature and concentration fields decrease for the enhance values of Pr and Le, respectively. Physically, the higher values of Prandtl number reduce the thermal diffusivity of the fluid and increasing values of Le decrease the mass diffusion coefficient. Thus, in result

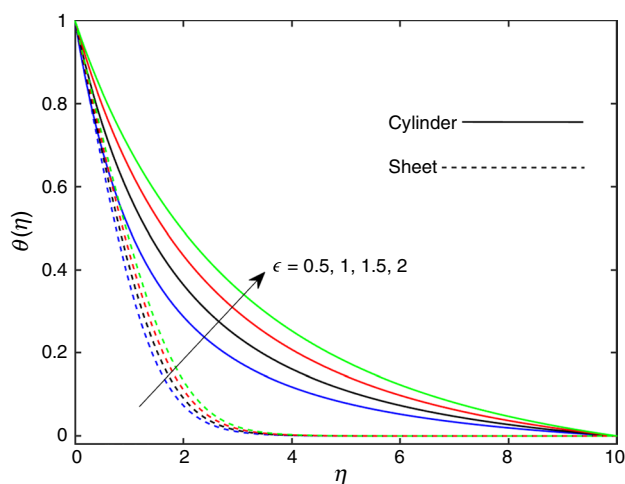


Fig. 7 The temperature profile via small thermal conductivity parameter  $\epsilon$

**Table 1** Numerical values of  $-f''(0)$  for different values of  $\beta_1$  when  $\alpha = S = 0$

| $\beta_1$ | $-f''(0)$ |           |           |                 |               |
|-----------|-----------|-----------|-----------|-----------------|---------------|
|           | Ref. [32] | Ref. [33] | Ref. [34] | Present (bvp4c) | Present (HAM) |
| 0.0       | 1.000000  | 1.000000  | 1.000000  | 1.000000        | 1.000000      |
| 0.1       |           |           | 1.026183  | 1.026190        | 1.026166      |
| 0.2       | 1.051948  | 1.051889  | 1.051889  | 1.051892        | 1.051866      |
| 0.3       |           |           | 1.077125  | 1.077127        | 1.075466      |
| 0.4       | 1.101850  | 1.101903  | 1.101903  | 1.101903        | 1.101880      |
| 0.5       |           |           | 1.126235  | 1.126234        | 1.125678      |
| 0.6       | 1.150163  | 1.150137  | 1.150137  | 1.150136        | 1.150144      |
| 0.7       |           |           | 1.173624  | 1.173623        | 1.173629      |
| 0.8       | 1.196692  | 1.196711  | 1.196711  | 1.196709        | 1.196455      |
| 0.9       |           |           | 1.219414  | 1.219413        | 1.219419      |
| 1.0       |           |           | 1.241747  | 1.241741        | 1.124567      |

heat and mass transfer decrease in the fluid. The thermal conductivity parameter  $\epsilon$  boost up the heat transfer rate of the fluid and thus in consequence the temperature field enhances as shown in Fig. 7. A comparison is given in Table 1 for reduced  $-f''(0)$  with varying values of  $\beta_1$  which assure the validation of our results. Table 2 is provided for the numerical values of thermal and solutal gradients at the surface of cylinder with varying values of pertinent parameters. It is noted that both gradients decrease with higher values of unsteadiness parameter and increase for Prandtl and Lewis numbers, respectively.

**Table 2** Numerical values of  $-\theta'(0)$  and  $-\phi'(0)$  in the limiting case for  $\beta_1 = \beta_c = 0$  and  $\alpha = 1$

| $S$ | $\beta_1$ | $M$ | $\epsilon$ | Pr  | Le  | $-\theta'(0)$ | $-\phi'(0)$ |
|-----|-----------|-----|------------|-----|-----|---------------|-------------|
| 0.1 | 0.1       | 01  | 0.1        | 6.5 | 6.5 | 1.919590      | 5.034541    |
| 0.2 |           |     |            |     |     | 1.820360      | 4.858232    |
| 0.3 |           |     |            |     |     | 1.709981      | 4.671831    |
| 0.4 |           |     |            |     |     | 1.586012      | 4.473812    |
| 0.1 | 0.1       | 01  | 0.1        | 6.5 | 6.5 | 1.925401      | 5.034541    |
|     | 0.3       |     |            |     |     | 1.922490      | 4.995886    |
|     | 0.5       |     |            |     |     | 1.919592      | 4.958616    |
|     | 0.7       |     |            |     |     | 1.916850      | 4.922654    |
| 0.1 | 0.1       | 01  | 0.1        | 6.5 | 6.5 | 1.919501      |             |
|     |           | 02  |            |     |     | 1.856914      |             |
|     |           | 03  |            |     |     | 1.799712      |             |
|     |           | 04  |            |     |     | 1.748013      |             |
| 0.1 | 0.1       | 01  | 0.1        | 6.5 | 6.5 | 1.919591      | 5.043821    |
|     |           |     | 0.2        |     |     | 1.825890      | 5.041512    |
|     |           |     | 0.3        |     |     | 1.741672      | 5.039201    |
|     |           |     | 0.4        |     |     | 1.665377      | 5.036881    |
| 0.1 | 0.1       | 01  | 0.1        | 02  | 6.5 | 1.141467      |             |
|     |           |     |            | 04  |     | 1.508042      |             |
|     |           |     |            | 06  |     | 1.842103      |             |
|     |           |     |            | 08  |     | 2.138361      |             |
| 0.1 | 0.1       | 01  | 0.1        | 6.5 | 02  |               | 2.799817    |
|     |           |     |            |     | 04  |               | 3.957422    |
|     |           |     |            |     | 06  |               | 4.837691    |
|     |           |     |            |     | 08  |               | 5.577224    |



## Final remarks

The final conclusions have been drawn for the problem of 2D unsteady flow of Maxwell fluid over the stretched cylinder. The Cattaneo–Christov theory is employed for heat and mass transport mechanisms. The thermal conductivity of fluid is assumed to be variable (temperature dependent). The following conclusions are drawn

- A similar manner is reported for flow, thermal and concentration fields for varying curvature parameter  $\alpha$ .
- Maxwell parameter  $\beta_1$  declines the flow field but it boosts up the thermal and concentration distributions.
- The heat and mass transport decreases with higher values of thermal and mass relaxation parameters  $\beta_t$  and  $\beta_c$ , respectively.
- The thermal diffusivity decreases for higher Prandtl number  $Pr$  and thus the transport of thermal energy in fluid is lower.

## References

1. Cattaneo C. Sulla conduzione del calore. *Atti Semin Mat Fis Univ Modena Rerrio Emilia*. 1948;3:83–101.
2. Christov CI. On a higher-gradient generalization of Fourier's law of heat conduction. In *AIP Conference Proceedings 2007* (Vol. 946, pp. 11–22).
3. Yousif MA, Ismael HF, Abbas T, Ellahi R. Numerical study of momentum and heat transfer of MHD Carreau nanofluid over exponentially stretched plate with internal heat source/sink and radiation. *Heat Transf Res*. 2019;50(7):649–58.
4. Sarafraz MM, Pourmehran O, Yang B, Arjomandi M, Ellahi R. Pool boiling heat transfer characteristics of iron oxide nanosuspension under constant magnetic field. *Int J Therm Sci*. 2020;147:106131.
5. Han S, Zheng L, Li C, Zhang X. Coupled flow and heat transfer in viscoelastic fluid with Cattaneo–Christov heat flux model. *Appl Math Lett*. 2014;38:87–93.
6. Upadhyaya SM, Mahesha, Raju CSK. Cattaneo–Christov heat flux model for magnetohydrodynamic flow in a suspension of dust particles towards a stretching sheet. *Nonlinear Eng*. 2018;7:237–46.
7. Khan WA, Irfan M, Khan M. An improved heat conduction and mass diffusion models for rotating flow of an Oldroyd-B fluid. *Results Phys*. 2017;7:3583–9.
8. Ibrahim W. Three dimensional rotating flow of Powell–Eyring nanofluid with non-Fourier's heat flux and non-Fick's mass flux theory. *Results Phys*. 2018;8:569–77.
9. Farooq M, Ahmad S, Javed M, Anjum A. Analysis of Cattaneo–Christov heat and mass fluxes in the squeezed flow embedded in porous medium with variable mass diffusivity. *Results Phys*. 2017;7:3788–96.
10. Alamri SZ, Khan AA, Azeed M, Ellahi R. Effects of mass transfer on MHD second grade fluid towards stretching cylinder: a novel perspective of Cattaneo–Christov heat flux model. *Phys Lett A*. 2019;383:276–81.
11. Ahmed J, Khan M, Ahmad L. Effectiveness of homogeneous-heterogeneous reactions in Maxwell fluid flow between two spiraling disks with improved heat conduction features. *J Therm Anal Calorim*. 2019;. <https://doi.org/10.1007/s10973-019-08712-9>.
12. Saleem S, Awais M, Nadeem S, Sandeep N, Mustafa MT. Theoretical analysis of upper-convected Maxwell fluid flow with Cattaneo–Christov heat flux model. *Chin J Phys*. 2017;55:1615–25.
13. Reddy GK, Yarrakula K, Raju CSK. Mixed convection analysis of variable heat source/sink on MHD Maxwell, Jeffrey, and Oldroyd-B nanofluids over a cone with convective conditions using Buongiorno's model. *J Therm Anal Calorim*. 2018;. <https://doi.org/10.1007/s10973-018-7115-0>.
14. Ellahi R, Zeeshan A, Shehzad N, Alamri SZ. Structural impact of kerosene-Al<sub>2</sub>O<sub>3</sub> nanoliquid on MHD Poiseuille flow with variable thermal conductivity: application of cooling process. *J Mol Liq*. 2018;264:607–15.
15. Tibullo V, Zampoli V. A uniqueness result for the Cattaneo–Christov heat conduction model applied to incompressible fluids. *Mech Res Commun*. 2011;38:77–9.
16. Bhattacharyya A, Seth GS, Kumar R. Simulation of Cattaneo–Christov heat flux on the flow of single and multi-walled carbon nanotubes between two stretchable coaxial rotating disks. *J Therm Anal Calorim*. 2019;. <https://doi.org/10.1007/s10973-019-08644-4>.
17. Ramadevi B, Kumar KA, Sugunamma V. Magnetohydrodynamic mixed convective flow of micropolar fluid past a stretching surface using modified Fourier's heat flux model. *J Therm Anal Calorim*. 2019;. <https://doi.org/10.1007/s10973-019-08477-1>.
18. Kumar KA, Sugunamma V, Sandeep N. Influence of viscous dissipation on MHD flow of micropolar fluid over a slendering stretching surface with modified heat flux model. *J Therm Anal Calorim*. 2019;. <https://doi.org/10.1007/s10973-019-08694-8>.
19. Asadollahi A, Esfahani JA, Ellahi R. Evacuating liquid coatings from a diffusive oblique fin in micro-/mini-channels. *J Therm Anal Calorim*. 2019;138:255–63.
20. Rashidi S, Eskandarian M, Mahian O, Poncet S. Combination of nanofluid and inserts for heat transfer enhancement. *J Therm Anal Calorim*. 2019;135(1):437–60.
21. Khan LA, Raza M, Mir NA, Ellahi R. Effects of different shapes of nanoparticles on peristaltic flow of MHD nanofluids filled in an asymmetric channel. *J Therm Anal Calorim*. 2019;. <https://doi.org/10.1007/s10973-019-08348-9>.
22. Raju CSK, Sandeep N, Malvandi A. Free convective heat and mass transfer of MHD non-Newtonian nanofluids over a cone in the presence of non-uniform heat source/sink. *J Mol Liq*. 2016;221:108–15.
23. Hsiao KL. Combined electrical MHD heat transfer thermal extrusion system using Maxwell fluid with radiative and viscous dissipation effects. *Appl Therm Eng*. 2017;112:1281–8.
24. Hsiao KL. To promote radiation electrical MHD activation energy thermal extrusion manufacturing system efficiency by using Carreau–Nanofluid with parameters control method. *Energy*. 2017;130:486–99.
25. Ahmed J, Khan M, Ahmad L. Stagnation point flow of Maxwell nanofluid over a permeable rotating disk with heat source/sink. *J Mol Liq*. 2019;287:110853.
26. Moshkin NP, Pukhnachev VV, Bozhkov YD. On the unsteady, stagnation point flow of a Maxwell fluid in 2D. *Int J Non-Linear Mech*. 2019;116:32–8.
27. Hsiao KL. Stagnation electrical MHD nanofluid mixed convection with slip boundary on a stretching sheet. *Appl Therm Eng*. 2016;98:850–61.

28. Hsiao KL. Micropolar nanofluid flow with MHD and viscous dissipation effects towards a stretching sheet with multimedia feature. *Int J Heat Mass Transf.* 2017;112:983–90.
29. Saif RS, Hayat T, Ellahi R, Muhammad T, Alsaedi T. Darcy–Forchheimer flow of nanofluid due to a curved stretching surface. *Int J Numer Method Heat Fluid Flow.* 2019;29(1):2–20.
30. Ahmed Z, Nadeem S, Saleem S, Ellahi R. Numerical study of unsteady flow and heat transfer CNT-based MHD nanofluid with variable viscosity over a permeable shrinking surface. *Int J Numer Methods Heat Fluid Flow.* 2019;29(12):4607–23.
31. Rajagopal KR. A note on novel generalizations of the Maxwell fluid model. *Int J Non-Linear Mech.* 2012;47(1):72–6.
32. Abel MS, Tawade JV, Nandeppanavar MM. MHD flow and heat transfer for the upper-convected Maxwell fluid over a stretching sheet. *Meccanica.* 2012;47:385–93.
33. Waqas M, Khan MI, Hayat T, Alsaedi A. Stratified flow of an Oldroyd-B nanoliquid with heat generation. *Results Phys.* 2017;7:2489–96.
34. Irfan M, Khan M, Khan WA. Impact of homogeneous-heterogeneous reactions and non-Fourier heat flux theory in Oldroyd-B fluid with variable conductivity. *J Braz Soc Mech Sci Eng.* 2019;. <https://doi.org/10.1007/s40430-019-1619-9>.

**Publisher's Note** Springer Nature remains neutral with regard to jurisdictional claims in published maps and institutional affiliations.